Angewandte Chemie
Eine Zeitschrift der Gesellschaft Deutscher Chemiker

Supporting Information

69451 Weinheim, Germany

Multiple Paramagnetic Effects through a Tagged Reporter Protein**

*Aldo R. Camacho-Zarco, Francesca Munari, Melanie Wegstroth, Wei-Min Liu, Marcellus Ubbink, Stefan Becker, and Markus Zweckstetter**

anie_201408615_sm_miscellaneous_information.pdf

Supporting information

Contents

Experimental methods

Homo sapiens ubiquitin, *Escherichia coli* MBP and the PDZ domain of homo sapiens Erbin (residues 1273-1371) were produced recombinantly and purified as described previously.[1] Production of CLaNP-5 as well as the selection and tagging of PDZ double cysteine mutants was performed as described previously[2]. Briefly, the residues selected to produce the 6 double cysteine mutants are located at the surface, their Cα atoms are 6-10 Å apart and their side chains point in the same direction to the solvent. A 10-fold excess of dithiotreitol (DTT) was added to a 0.5 mM solution of any PDZ double mutant in 20 mM sodium phosphate pH 7.0 and incubated on ice for 1 h to reduce their cysteine residues. A Superdex 75 column was used to eliminate the excess of DTT. Immediately after that, 10 equivalents of Ln-CLaNP-5 were added to a 60 μM solution of the reduced PDZ in degassed buffer containing 20 mM sodium phosphate pH 7.0 with 150 mM NaCl and stirred on ice for 4 hours. The excess of CLaNP-5 and dimeric products of PDZ were eliminated using a Superdex 75 column. HPLC-MS analysis of the reactions was performed in order to confirm the modification and determine the yield of the reactions. For example, PDZ-1 (theoretical mass 11482.1 Da) yielded a mass of 11482.3 Da, which indicates that the lanthanide tag is attached to both of the cysteine residues.

NMR samples used to acquire paramagnetic data of $MBP^{TGWETWV}$ contained 50 mM NaCl, 2 mM β-cyclodextrin, 20 mM phosphate buffer pH 7.2, 10% D_2O, 0.25 mM of $MBP^{TGWETWV}$ and 0.5 mM of CLaNP-5 tagged PDZ, loaded with either Lu^{3+} of Tm^{3+}. Paramagnetic NMR data were acquired on Bruker Avance 800 and 900 MHz spectrometers using HSQC-TROSY interleaved experiments[3] at 310 K. To decrease signal overlap, a 3D HNCO-based experiment[4] was recorded at a 700 MHz Bruker spectrometer in addition. The sample used in this experiment contained 0.6 mM of $^{2}H,^{13}C,^{15}N$-$MBP^{TGWETWV}$ and 1.2 mM of CLaNP-5 tagged PDZ-1. The experimental conditions were the same ones used in the 2D experiments. Data were processed using NMRpipe[5] and analysed with Sparky[6]. The software PALES[7] was used to back-calculate RDCs and determine the alignment tensors using the MBP structure 1DMB[8], PDZ structure 1N7T[1a] and the ubiquitin 3D structure 1D3Z[1c]. In order to estimate the uncertainty in the determined alignment tensors, 1000 steps of the "structural noise Monte-Carlo method" were performed[9]. In short, this method consists in adding noise to the structure with a magnitude that matches the RMSD between observed and predicted RDCs. The extent of the alignment parameters obtained from these noise-corrupted structures (when using the coupling constants back-calculated for the original structure) represents a good measure of the uncertainty in the derived tensor. PCSs were fit to 3D structures using the software Numbat[10]. The transfer of assignments to the paramagnetic spectra was done manually, without running further experiments, as most of the pseudo contact shifts were smaller than 0.3 ppm.

^{15}N R_2 spin relaxation rates of unbound and PDZ-bound $MBP^{TGWETWV}$, wild -type ubiquitin and $ubiquitin^{TGWETWV}$ bound to PDZ were acquired using a CPMG TROSY-based experiment at 310 K, 600 MHz. $MBP^{TGWETWV}$ samples contained 0.4 mM of ^{2}H, ^{13}C, ^{15}N-$MBP^{TGWETWV}$, as well as 0.8 mM of wild-type PDZ in the case of the bound form. In the case of ubiquitin, relaxation experiments were measured on a sample containing 0.5 mM ^{15}N wild-type ubiquitin or ^{15}N-$ubiquitin^{TGWETWV}$ and 1 mM unlabelled wild-type PDZ (20 mM sodium phosphate buffer pH 6.5, 10% D_2O and 100 mM NaCl). Delay durations of 4, 8, 12, 16, 28 and 36 ms were used for the $MBP^{TGWETWV}$/PDZ complex; for free $MBP^{TGWETWV}$, relaxation delays of 4, 12, 28, 40, 52 and 80 ms were employed. For $ubiquitin^{TGWETWV}$ bound to PDZ, relaxation delays of 4, 20, 40, 80, 136 and 216 ms were used, while in case of wild-type ubiquitin the delays were set to 4, 36, 67, 99, 182 and 269 ms. R1ρ values of ^{15}N-$ubiquitin^{TGWETWV}$ bound to wild-type PDZ were obtained using relaxation delays of 8, 24, 48, 80, 120, 150, and 210 ms at 298 K.

Backbone chemical shifts of $MBP^{TGWETWV}$ bound to wild-type PDZ were confirmed and completed using TROSY-based triple-resonance experiments recorded on a sample of 0.6 mM ^{2}H, ^{13}C, ^{15}N-$MBP^{TGWETWV}$ in the presence of 1.2 mM wild-type PDZ. Backbone chemical shifts of $ubiquitin^{TGWETWV}$ bound to wild-type PDZ were obtained using standard triple-resonance experiments recorded on a 1.3 mM sample of ^{13}C, ^{15}N-$ubiquitin^{TGWETWV}$ in presence of wild-type PDZ at molar ratio of 1:2. To acquire paramagnetic data, a sample containing 0.2 mM of ^{15}N-$ubiquitin^{TGWETWV}$ and 0.4 mM of PDZ-1 was used. Band-selective decoupled (BSD) IPAP-HSQC experiments were recorded at 310 K[11]. For chemical shift perturbation analysis, chemical shifts of $ubiquitin^{TGWETWV}$/$MBP^{TGWETWV}$ bound to PDZ were compared to those of wild-type ubiquitin/MBP [1b]. Averaged, normalized $^{1}H/^{15}N$ chemical shift changes were calculated according to: $\Delta=\{[(\Delta H)^2 + (\Delta N/5)^2]\}^{1/2}$.

PRE distances were calculated from intensity ratios (assuming a Curie-spin relaxation mechanism) according to previously published procedures [12],[13]. In these calculations, it was taken into account that Tm^{3+} has a total angular magnetic quantum number J of 6 and its Landé g-factor (g_j) equals to 7/6 [14]. The program HYCUD was used to estimate the correlation time of $MBP^{TGWETWV}$ bound to PDZ (28.9 ns)[15].

Isothermal titration calorimetry experiments were done on a MicroCal ITC 200 microcalorimeter at 298 K. $Ubiquitin^{TGWETWV}$ and PDZ samples were extensively dialyzed against 20 mM sodium phosphate buffer pH 6.5, 100 mM NaCl. The sample cell contained 0.05 mM of $ubiquitin^{TGWETWV}$ and the injection syringe was filled with 0.8 mM PDZ protein. Experimental data were analyzed using the Microcal Origin software.

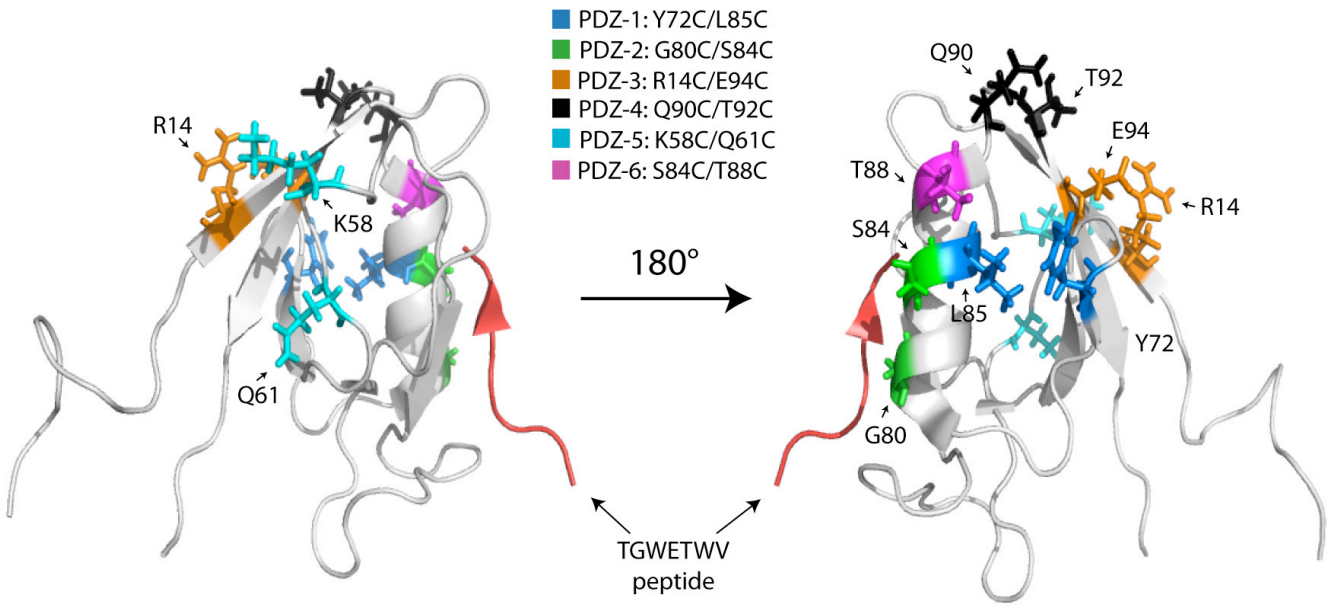

Figure S1. Localization of lanthanoid tagging sites in the Erbin PDZ domain. In order to attach the lanthanoid tag CLaNP-5, preloaded with Tm^{3+} or Lu^{3+}, six different double cysteine mutants were designed. The numbering corresponds to that of the 3D structure of PDZ in complex with the TGWETWV peptide, shown in red (PDB code: 1N7T).

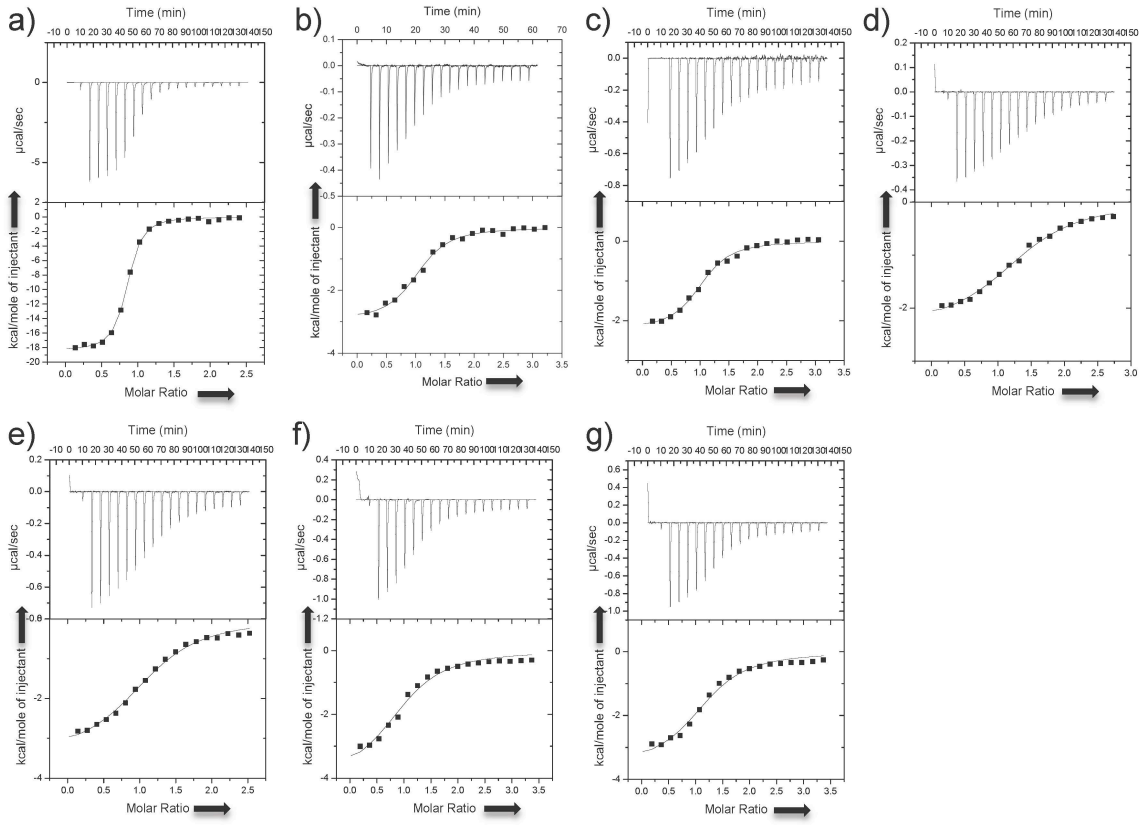

Figure S2. ITC curves of PDZ binding to MBP^{TGWETWV} or ubiquitin^{TGWETWV} The K_d constants reported in table S1 were determined from at least 2 independent experiments. a) and b) Binding of MBP^{TGWETWV} and ubiquitin^{TGWETWV} to wild-type PDZ. c) to g) Binding of ubiquitin^{TGWETWV} to PDZ-1, PDZ-2, PDZ-3, PDZ-5 and PDZ-6, respectively.

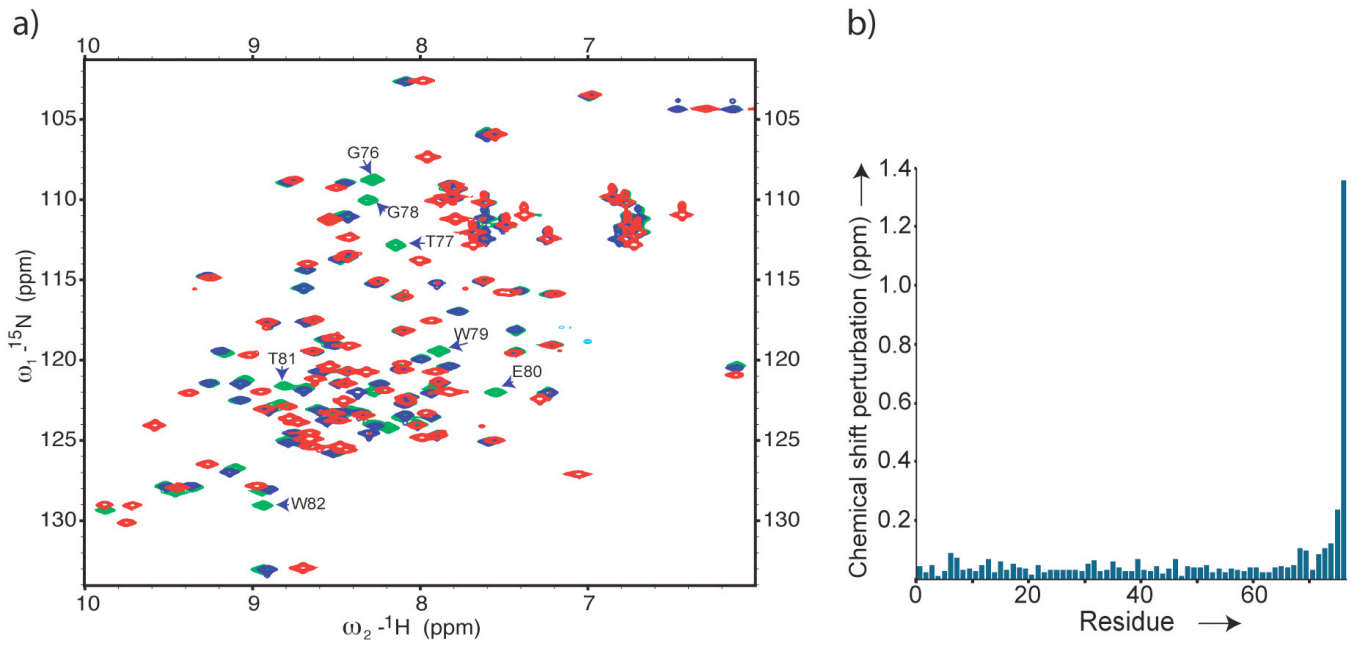

Figure S3. PDZ-binding to the C-terminal TGWETWV extension does not perturb the structure of wild-type ubiquitin. a) Superposition of ^{1}H-^{15}N HSQC spectra of wild-type ubiquitin (blue), unbound ubiquitin^{TGWETWV} (red) and ubiquitin^{TGWETWV} bound to wild-type PDZ (green). When PDZ is absent, the presence of the TGWETWV sequence at the C-terminus of ubiquitin produces a change in the chemical shift of several residues, probably because of a transient interaction of the peptide with the ubiquitin surface. This transient interaction is likely to be responsible for the lower affinity of PDZ to ubiquitin^{TGWETWV} when compared to MBP^{TGWETWV} (Table S1), which does not show similar chemical shift changes (Figure S6). Cross-peaks that belong to the C-terminal residues of ubiquitin^{TGWETWV} when bound to PDZ (green) are labelled. b) Averaged, normalized ^{1}H/^{15}N chemical shift changes between wild-type ubiquitin (BMRB entry: 17769) and ubiquitin^{TGWETWV} bound to PDZ-1 (which was tagged with CLaNP-5 and loaded with Lu^{3+}). Averaged, normalized ^{1}H/^{15}N chemical shift changes were calculated according to: $\Delta=\{[(\Delta H)^2 + (\Delta N/5)^2]\}^{1/2}$.

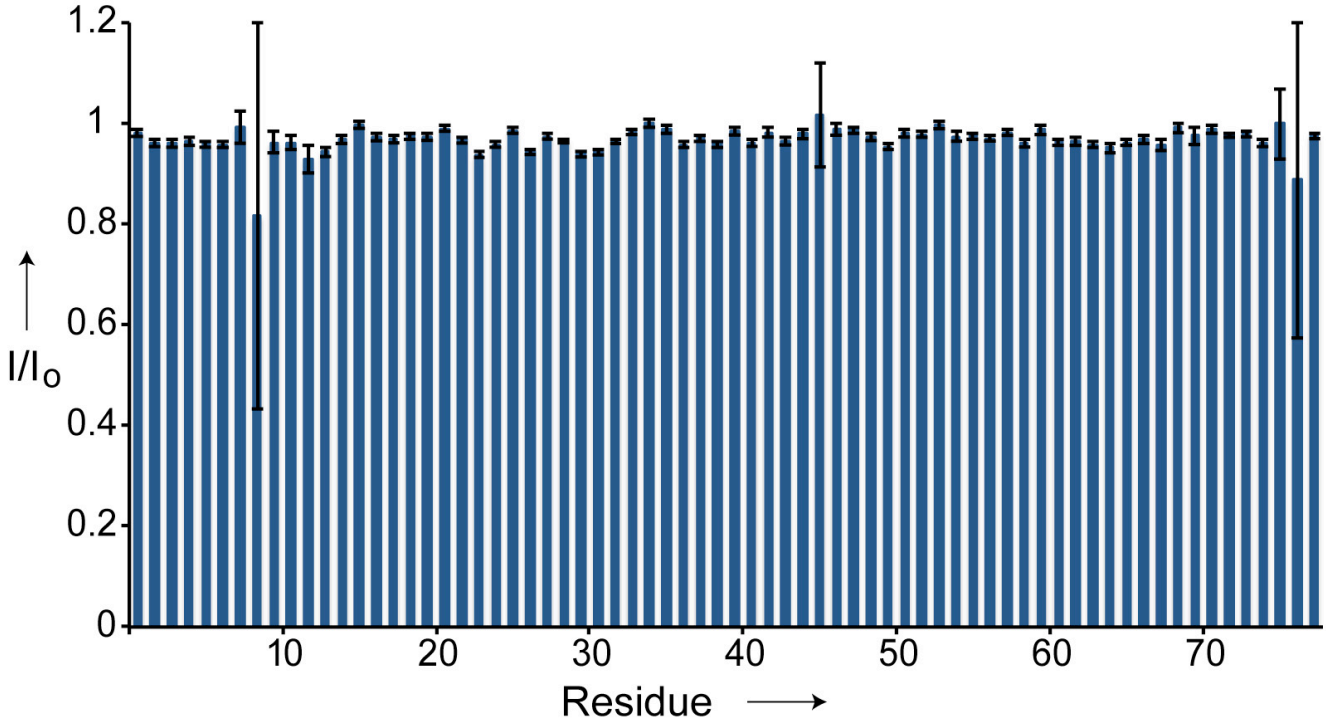

Figure S4. Ratio of NMR signal intensities in wild-type ubiquitin in the absence (I_0) and presence (I) of a two-fold excess of PDZ-6 (Tm^{3+}). Two samples containing 0.25 mM wild-type ubiquitin, one just with buffer and another containing in addition 0.5 mM PDZ-6 (tagged with CLaNP-5 and loaded with Tm^{3+}), were measured in identical conditions. Signal intensity ratios do not deviate from 1.0 indicating that excess PDZ does not perturb signal intensities in ubiquitin.

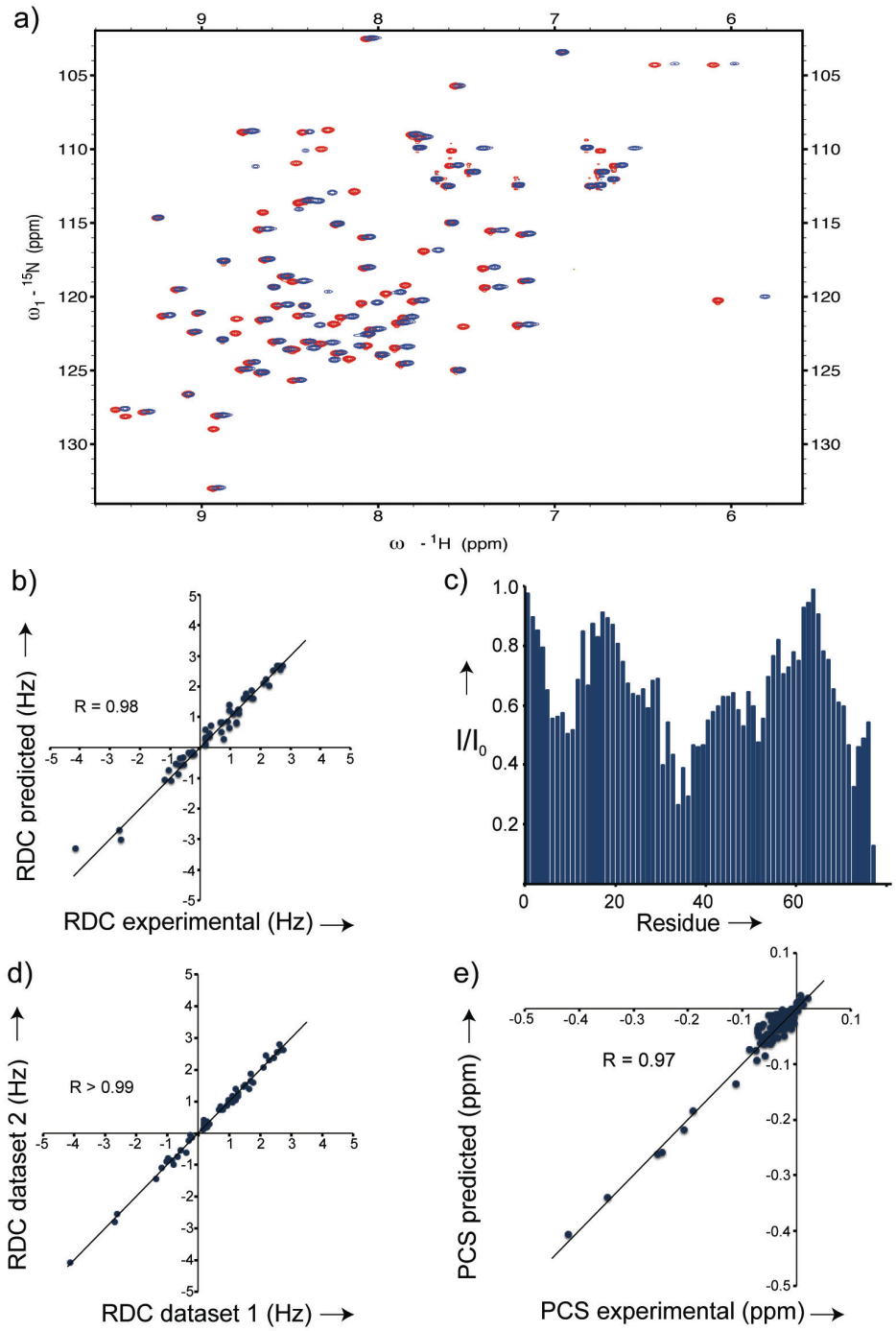

Figure S5. Paramagnetic effects in ubiquitin^{TGWETWV} bound to PDZ-1. For the diamagnetic and paramagnetic state, CLaNP-5 tagged PDZ-1 was preloaded with Lu^{3+} and Tm^{3+}, respectively. a) Superposition of the diamagnetic (red) and paramagnetic (blue) ^{1}H-^{15}N HSQC spectrum of ubiquitin^{TGWETWV} bound to PDZ-1. HSQC spectra were recorded at a ^{1}H Larmor frequency of 900 MHz. b) Comparison of experimental RDCs, which were determined using the BSD-IPAP HSQC pulse sequence[11] at a ^{1}H Larmor frequency of 600 MHz, with values back-calculated from ubiquitin's 3D structure (PDB code: 1D3Z) by singular value decomposition. c) Sequence-specific ratio of the signal intensity observed in the diamagnetic (I_0) and paramagnetic (I) HSQC spectrum shown in (a). d) Correlation of two RDC datasets acquired using the BSD-IPAP HSQC pulse sequence[11] at a ^{1}H Larmor frequency of 600 MHz. e) Experimental PCSs observed at a ^{1}H Larmor frequency of 800 MHz were fit to the 3D structure of ubiquitin (PDB code: 1D3Z) using the software Numbat. In all plots the straight line indicates y=x. Pearson's correlation factors, *R*, between experimental and back-calculated values are indicated.

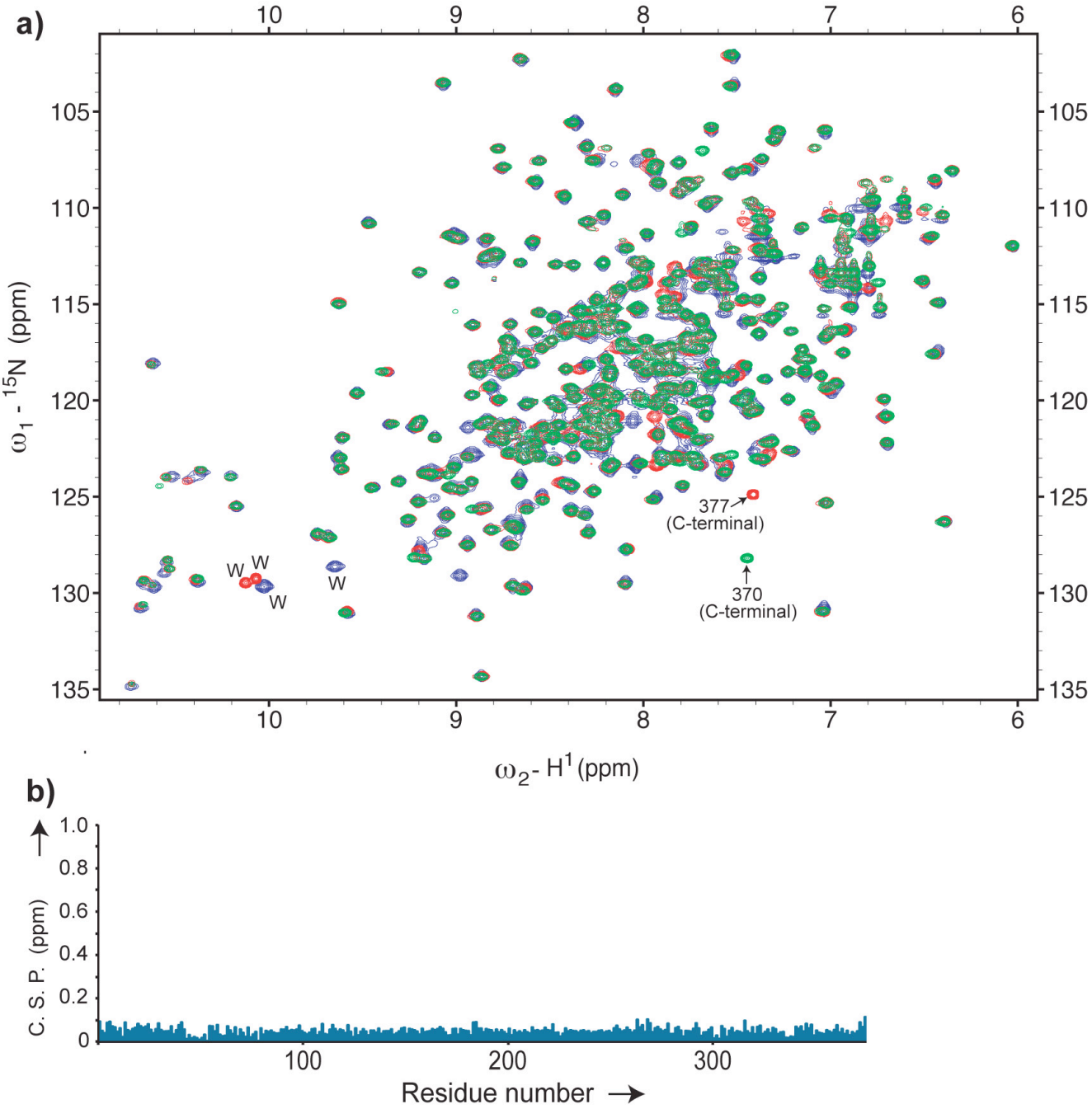

Figure S6. Chemical shifts in MBP^{TGWETWV} bound to wild-type PDZ. a) Superposition of ^{1}H-^{15}N HSQC spectra of wild-type MBP (green, 370 residues), unbound MBP^{TGWETWV} (red, 377 residues) and MBP^{TGWETWV} bound (blue) to PDZ-1, which had been tagged with CLaNP-5 and loaded with Lu^{3+} (added at a 2:1 molar excess). b) Averaged, normalized ^{1}H/^{15}N chemical shift changes between wild-type MBP and MBP^{TGWETWV} bound to wild-type PDZ. Averaged, normalized ^{1}H/^{15}N chemical shift changes were calculated according to: $\Delta=\{[(\Delta H)^2 + (\Delta N/5)^2]\}^{1/2}$.

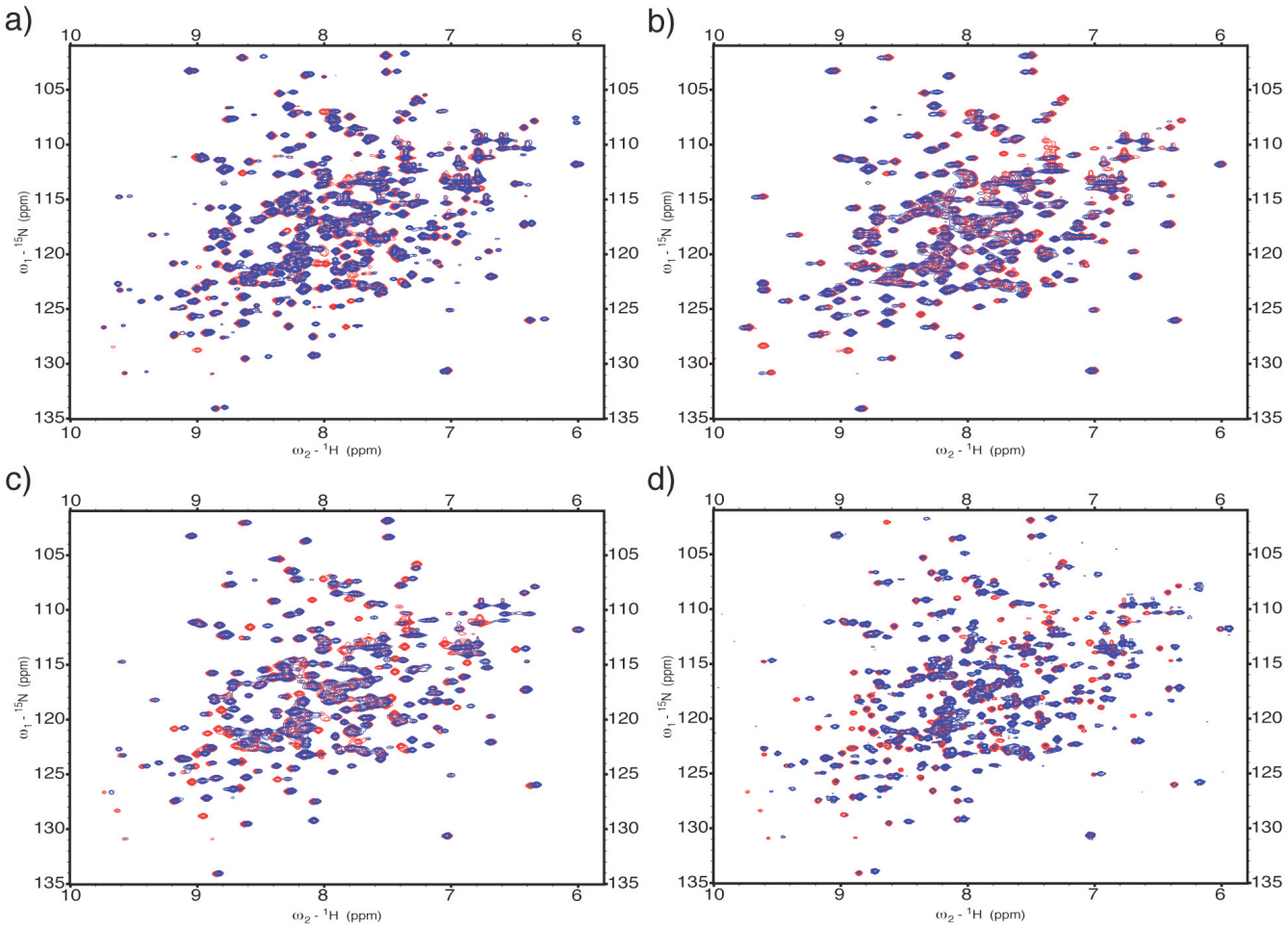

Figure S7. Superposition of ^{1}H-^{15}N HSQC spectra of ^{2}H, ^{15}N-MBP^{TGWETWV} bound to PDZ mutants in the diamagnetic (red) and paramagnetic state (blue). a) - d) PDZ-2, PDZ-3, PDZ-5 and PDZ-6, respectively, tagged with CLaNP-5 and loaded with either Lu^{3+} (red) or Tm^{3+}(blue).

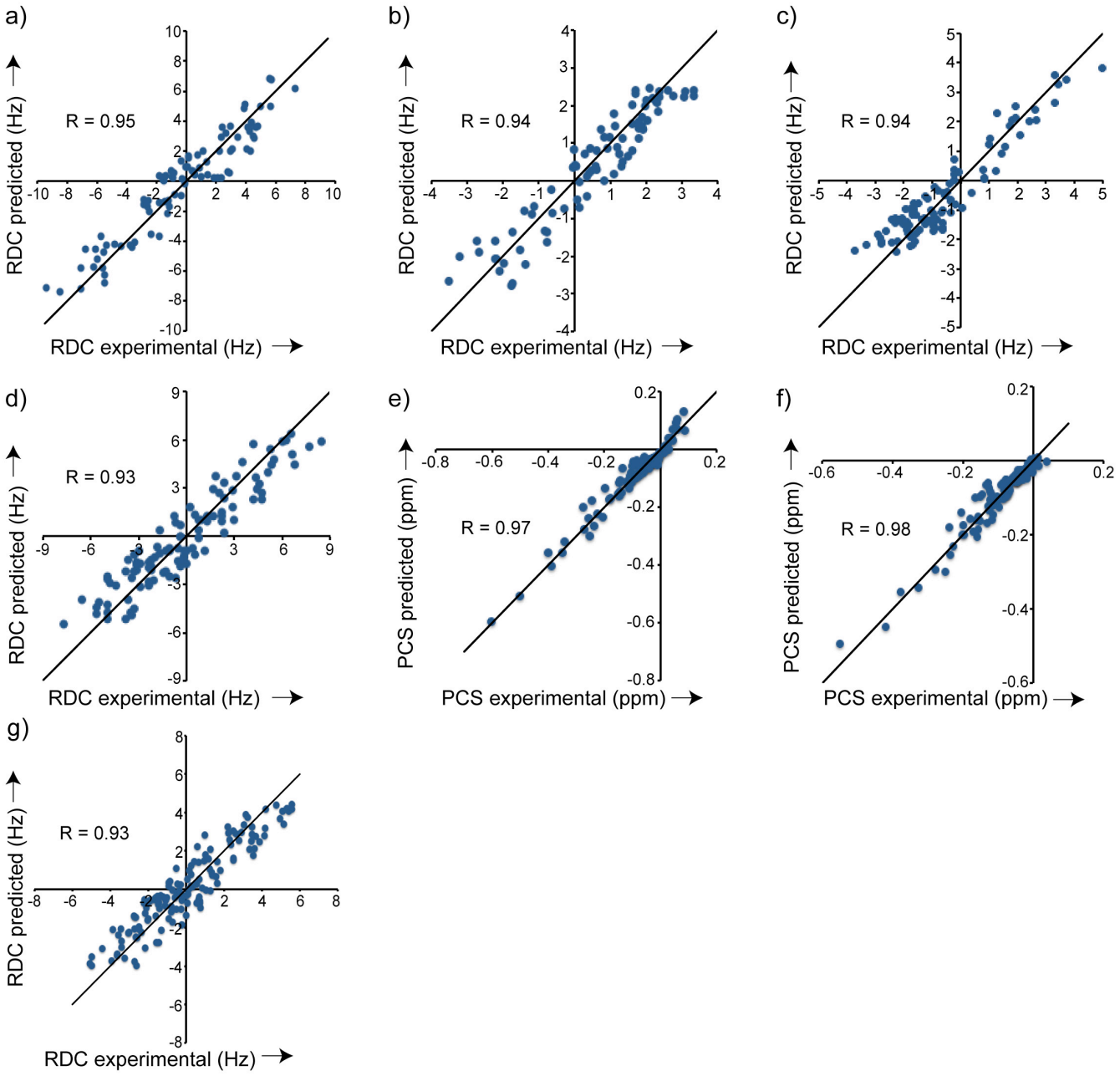

Figure S8. Comparison of experimental RDCs and PCSs observed in MBP^{TGWETWV} with values back-calculated from MBP's 3D structure. a) - d) Experimental N-H RDC observed in MBP^{TGWETWV} bound to CLaNP-5-tagged PDZ-1, PDZ-3, PDZ-5 and PDZ-6, respectively, were fit to MBP's 3D structure (PDB code: 1DMB) using singular value decomposition as implemented in the software PALES. Experiments were recorded at a ^{1}H Larmor frequency of 900 MHz. e) - f) Experimental H^{N} PCSs observed in MBP^{TGWETWV} bound to PDZ-1 and PDZ-6, respectively, were fitted to the same 3D structure using the program Numbat. g) Comparison of experimental N-H RDCs, which were measured by a 3D HNCO-based experiment[4] at a ^{1}H Larmor frequency of 700 MHz in MBP^{TGWETWV} bound to PDZ-1, with values back-calculated from MBP's 3D structure (PDB code: 1DMB). All data were recorded at 310 K. The line marks y=x. Pearson's correlation factors, *R*, between experimental and back-calculated values are indicated.

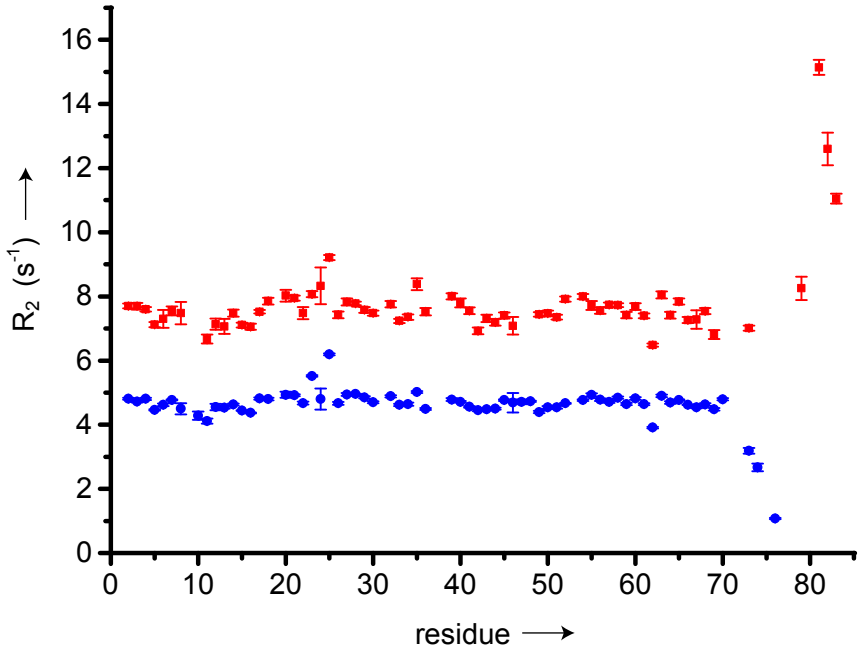

Figure S9. ^{15}N R2 spin-relaxation rates of wild-type ubiquitin (blue) and ubiquitin^{TGWETWV} bound to wild-type PDZ (red). The experiments were recorded at 310 K on a 600 MHz Bruker Avance spectrometer.

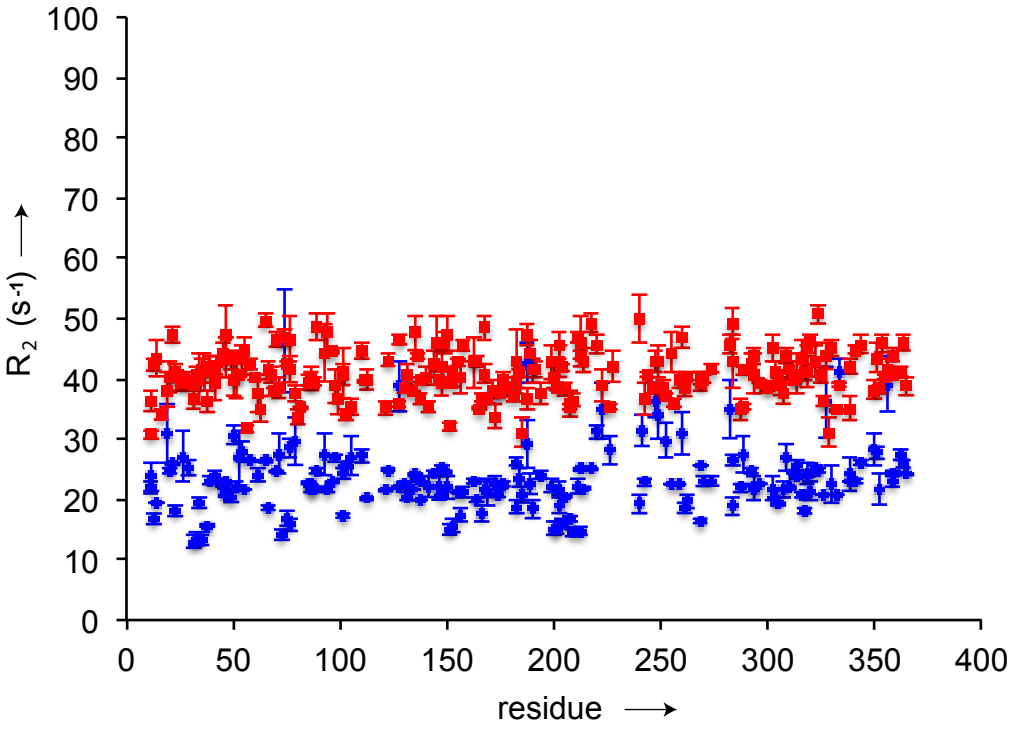

Figure S10. ^{15}N R2 spin-relaxation rates of unbound MBP^{TGWETWV} (blue) and MBP^{TGWETWV} bound to wild-type PDZ (red). The experiments were recorded at 310 K on a 600 MHz Bruker Avance spectrometer.

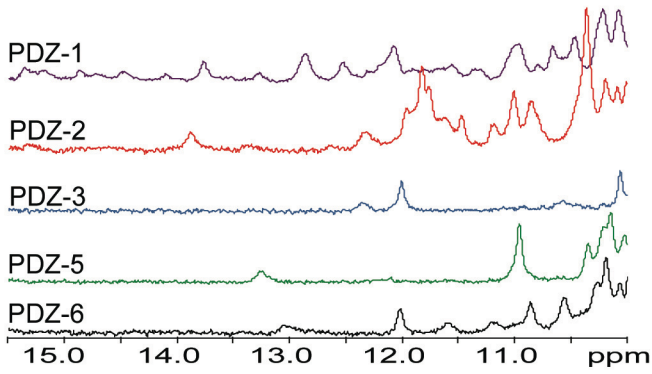

Figure S11. 1D ^{1}H spectra of PDZ mutants tagged with Tm^{3+}-preloaded CLaNP-5. Experiments were acquired at 310 K on a 700 MHz spectrometer. Solvent suppression was achieved by ^{1}H presaturation.

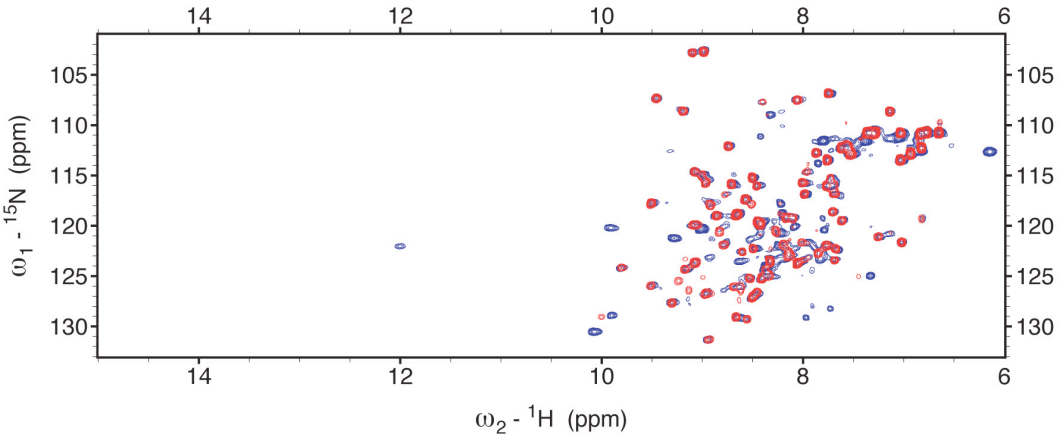

Figure S12. Superposition of diamagnetic (red) and paramagnetic (blue) ^{1}H-^{15}N HSQC spectra of PDZ-3. CLaNP-5 was loaded with Lu^{3+} (red) or Tm^{3+} (blue) prior to tagging of PDZ-3.

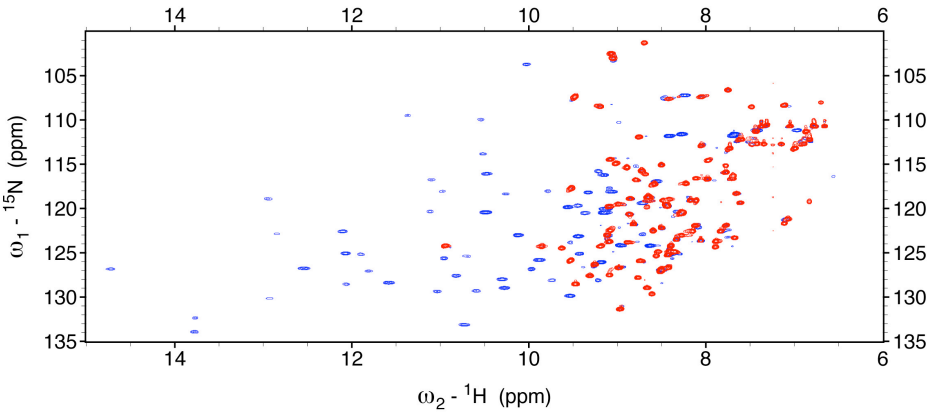

Figure S13. Superposition of diamagnetic (red) and paramagnetic (blue) ^{1}H-^{15}N HSQC spectra of PDZ-1 tagged with CLaNP-5. CLaNP-5 was loaded with Lu^{3+} (red) or Tm^{3+} (blue) prior to tagging of PDZ-1. Due to the large PCSs induced by the internal lanthanide tagging site, many resonances in the paramagnetic state are strongly shifted, requiring reassignment of PDZ-1 tagged with Tm^{3+}-CLaNP-5.

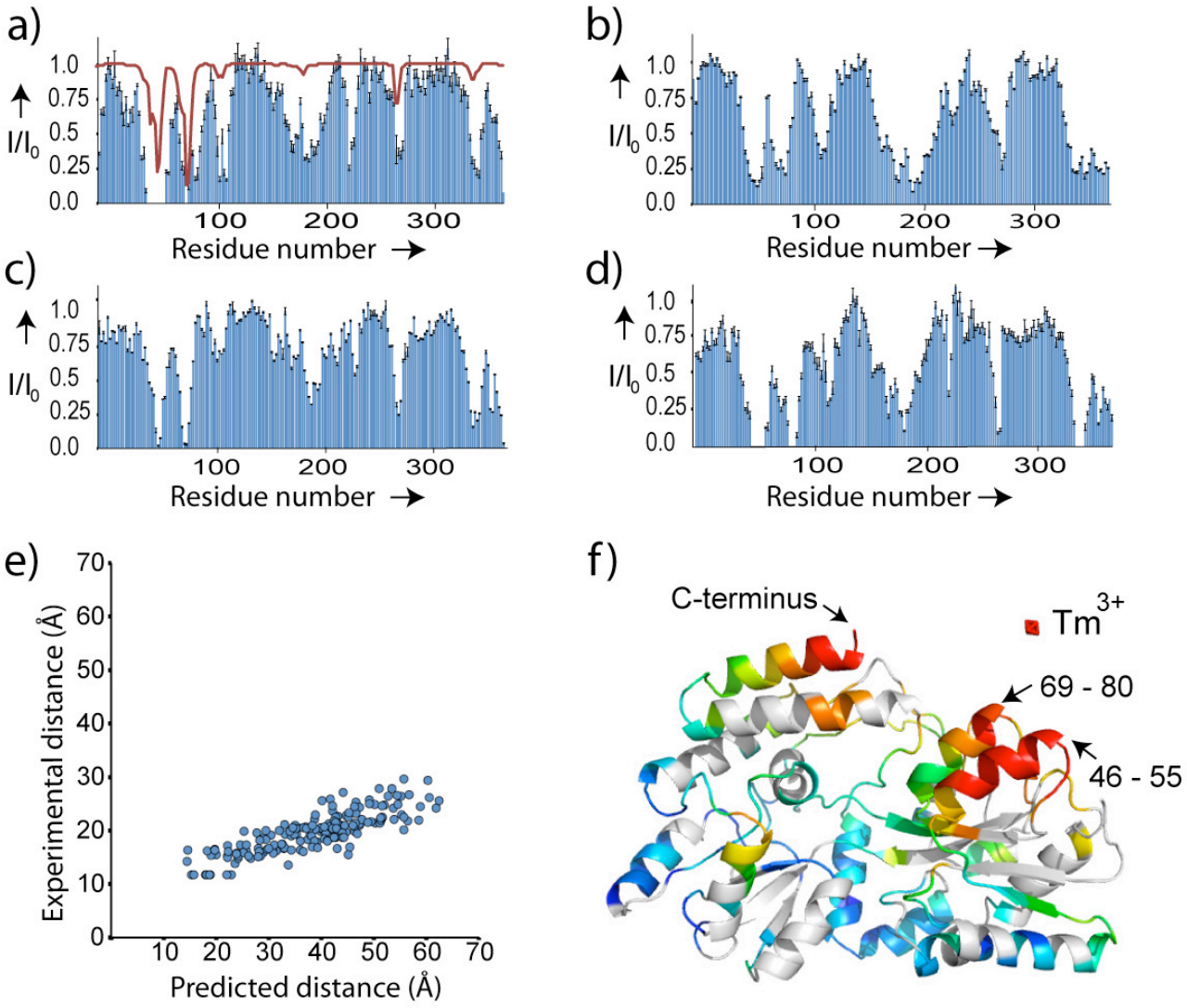

Figure S14. PRE profiles in MBP^{TGWETWV} upon addition of PDZ tagged with CLaNP-5 (Tm^{3+}). a) to d) PRE profiles (intensity rations) due to the addition of PDZ-1, PDZ-3, PDZ-5 and PDZ-6, respectively. Error bars were calculated on the basis of the signal-to-noise ratio in the NMR spectra. Only cross-peaks not strongly affected by signal overlap (also with respect to residual diamagnetic signals) were included into the analysis. The red line on the plot that corresponds to PDZ-1 indicates predicted intensity ratios obtained from the distance between the amide proton and the paramagnetic center (assuming Curie-spin relaxation), for which the position was determined from the experimentally observed ^{1}H and ^{15}N PCSs. e) Experimental PRE intensity ratios induced in MBP^{TGWETWV} by PDZ-1 were converted into distances between the amide proton and the paramagnetic center and compared to predicted distances derived from MPB's 3D structure (PDB code: 1DMB). f) PRE broadening induced by PDZ-1 was mapped onto MPB's 3D structure. From red (most affected, for example regions 46 - 55 and 69 - 80) to blue (unaffected), distance-dependent changes in signal intensity are shown. The PDZ recognition sequence TGWETWV is located at the C-terminus. The red sphere marks the position of the lanthanoid (derived from PCSs).

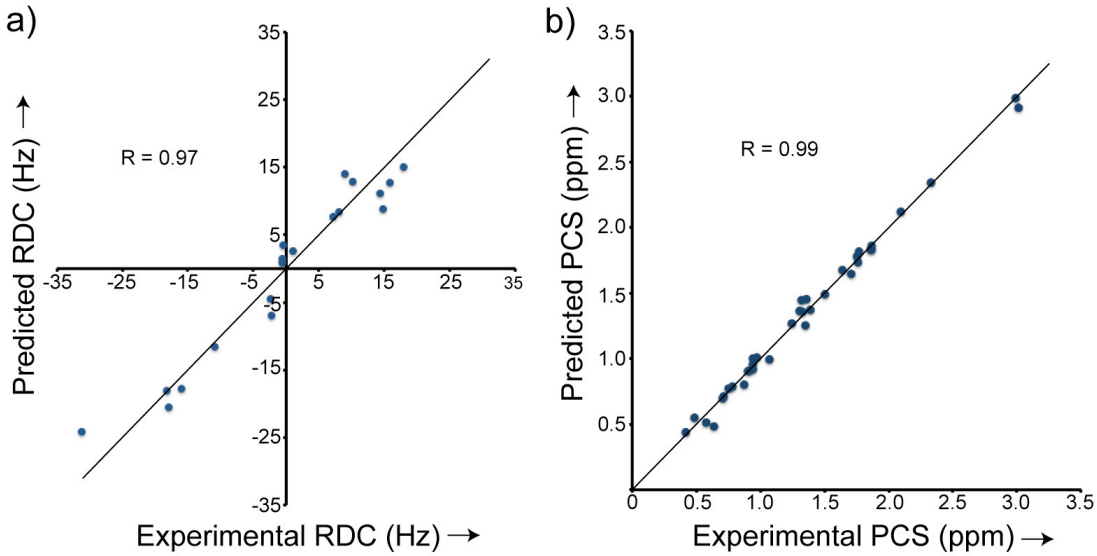

Figure S15. Comparison of RDCs and PCSs observed in CLaNP-5-tagged PDZ-1 with values back-calculated from the 3D structure of PDZ. a) Experimental RDCs were fit to the 3D structure of Erbin PDZ (PDB code: 1N7T) using the software PALES. Only a small number of RDCs could be analysed due to strong paramagnetic signal broadening (Figure S13). b) Experimental PCSs were fit to the 3D structure of Erbin PDZ (PDB code: 1N7T) using the software Numbat. Experiments were acquired at a ^{1}H Larmor frequency of 900 MHz. The straight line indicates y=x.

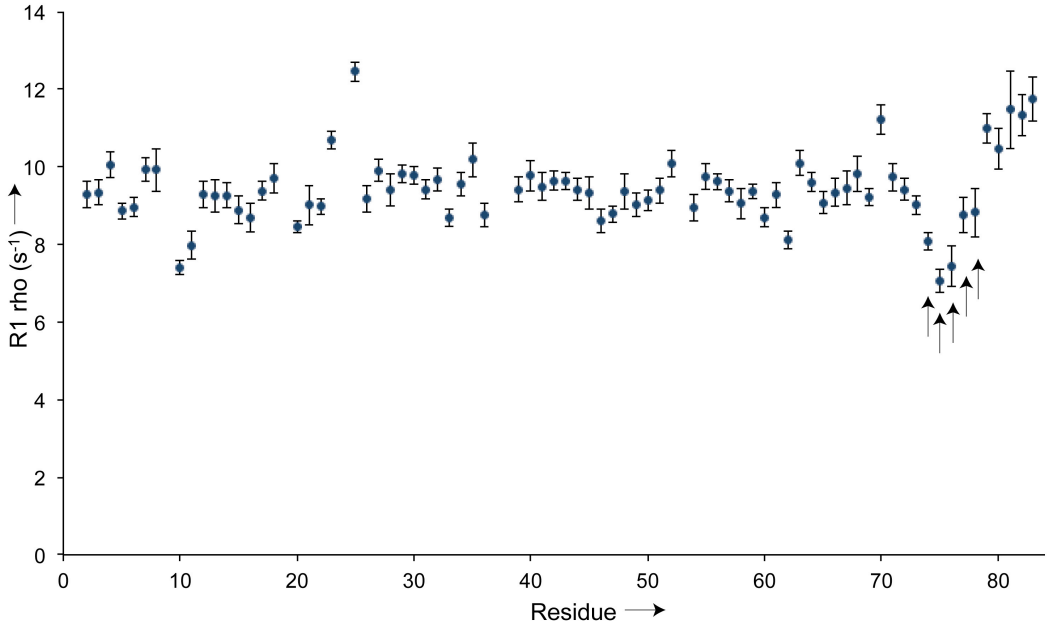

Figure S16. ^{15}N $R_1\rho$ spin-relaxation rates of ubiquitin^{TGWETWV} bound to wild-type PDZ. The black arrows indicate the last three residues of ubiquitin and the first two residues of the PDZ recognition sequence TGWETWV. These five residues constitute the flexible linker of the complex. Experiments were recorded at 298 K on a 600 MHz Bruker Avance spectrometer.

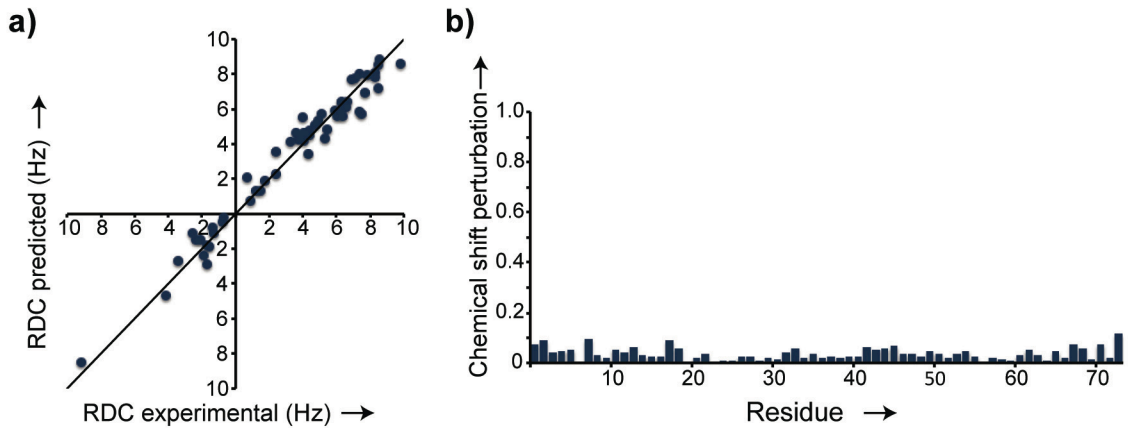

Figure S17. RDCs and chemical shift changes in ubiquitin^{WETWV} bound to PDZ-1. a) PDZ-1 was added to a mutant ubiquitin, in which G76 was deleted and the PDZ recognition sequence was shortened by two residues to WETWV. RDCs were obtained at a ^{1}H Larmor frequency of 900 MHz (37 °C). RDCs were fitted to ubiquitin's 3D structure (PDB code: 1D3Z) using singular value decomposition as implemented in the program PALES. b) Averaged, normalized ^{1}H/^{15}N chemical shift changes between ubiquitin^{WETWV} and ubiquitin^{TGWETWV}.

Table S1. Dissociation constants of different PDZ mutants for TGWETWV-fused proteins.

PDZ construct	Protein	K_d (μM)
PDZ wild-type	MBP	0.81 ± 0.03
PDZ wild-type	Ubiquitin	4.1 ± 0.6
PDZ-1	Ubiquitin	5.0 ± 1.5
PDZ-2	Ubiquitin	6.1 ± 0.6
PDZ-3	Ubiquitin	14.8 ± 1.3
PDZ-5	Ubiquitin	6.2 ± 1.2
PDZ-6	Ubiquitin	4.8 ± 0.5

Table S2. Tagging efficiency of different PDZ mutants. After the tagging reaction, tagging efficiency of each mutant was determined by HPLC-MS analysis.

PDZ mutant	% Tagging
PDZ-1	95
PDZ-2	42
PDZ-3	67
PDZ-5	95
PDZ-6	80

Table S3. Parameters of alignment tensors transmitted to $MBP^{TGWETWV}$ by PDZ mutants tagged with CLaNP-5. Alignment tensors and Q-values were obtained by best-fit of experimental RDCs to the 3D structure 1DMB using the software PALES.

PDZ mutant	A_a (10^{-4})	A_r (10^{-4})	α^c	β^c	γ^c	Q value
PDZ-1[a]	-3.0 ± 0.2	-1.7 ± 0.2	-13.5	-17.9	37.2	0.23
PDZ-2[b]	-3.8 ± 0.4	-1.8 ± 0.3	42.9	239.1	-8.4	0.26
PDZ-3[a]	-1.2 ± 0.1	-0.5 ± 0.1	78.9	-32.8	251.1	0.29
PDZ-5[b]	1.6 ± 0.1	0.3 ± 0.1	111.1	-41.1	-42.1	0.24
PDZ-6[b]	2.8 ± 0.1	1.2 ± 0.1	90.8	22.0	-1.1	0.28

[a] Measured at 800 MHz or [b] 900 MHz; [c] Euler angles.

Table S4. Alignment tensor of CLaNP-5-tagged PDZ-1 as determined from RDCs. Spectra were recorded at 310 K on a Bruker Avance 900 MHz spectrometer. RDCs were fit to the 3D structure of PDZ (PDB code: 1N7T) using the software PALES[7].

PDZ-1	Parameters
A_a (10^{-3})	-1.1
A_r (10^{-4})	-2.4
α	24.3
β	-43.5
γ	79.5
Q value	0.19

Table S5. Number of paramagnetic cross-peaks assigned on two-dimensional ^{1}H-^{15}N TROSY-HSQC spectra of MBP^{TGWETWV}. The different PDZ mutants were tagged with CLaNP-5 loaded with Tm^{3+}. These were added to ^{2}H, ^{15}N-MBP^{TGWETWV}. 229 isolated cross-peaks were assigned at most in the diamagnetic versions (Lu^{3+}) of these spectra.

Mutants	# Peaks
PDZ-1	209
PDZ-2	211
PDZ-3	213
PDZ-5	227
PDZ-6	206

References

[1] a) N. J. Skelton, M. F. T. Koehler, K. Zobel, W. L. Wong, S. Yeh, M. T. Pisabarro, J. P. Yin, L. A. Lasky, S. S. Sidhu, *J Biol Chem* **2003**, *278*, 7645-7654; b) K. H. Gardner, X. C. Zhang, K. Gehring, L. E. Kay, *J Am Chem Soc* **1998**, *120*, 11738-11748; c) S. Vijaykumar, C. E. Bugg, W. J. Cook, *J Mol Biol* **1987**, *194*, 531-544.

[2] P. H. J. Keizers, A. Saragliadis, Y. Hiruma, M. Overhand, M. Ubbink, *J Am Chem Soc* **2008**, *130*, 14802-14812.

[3] G. Kontaxis, G. M. Clore, A. Bax, *J Magn Reson* **2000**, *143*, 184-196.

[4] P. Permi, P. R. Rosevear, A. Annila, *J Biomol NMR* **2000**, *17*, 43-54.

[5] F. Delaglio, S. Grzesiek, G. W. Vuister, G. Zhu, J. Pfeifer, A. Bax, *J Biomol NMR* **1995**, *6*, 277-293.

[6] G. T. D. a. K. D. G., *University of California, San Francisco.*

[7] M. Zweckstetter, *Nat Protoc* **2008**, *3*, 679-690.

[8] A. J. Sharff, L. E. Rodseth, F. A. Quiocho, *Biochemistry* **1993**, *32*, 10553-10559.

[9] M. Zweckstetter, A. Bax, *J Biomol NMR* **2002**, *23*, 127-137.

[10] C. Schmitz, M. J. Stanton-Cook, X. C. Su, G. Otting, T. Huber, *J Biomol NMR* **2008**, *41*, 179-189.

[11] L. S. Yao, J. F. Ying, A. Bax, *J Biomol NMR* **2009**, *43*, 161-170.

[12] J. L. Battiste, G. Wagner, *Biochemistry* **2000**, *39*, 5355-5365.

[13] a) G. Pintacuda, A. Kaikkonen, G. Otting, *J Magn Reson* **2004**, *171*, 233-243; b) G. M. Clore, J. Iwahara, *Chem Rev* **2009**, *109*, 4108-4139.

[14] J. Koehler, J. Meiler, *Prog Nucl Mag Res Sp* **2011**, *59*, 360-389.

[15] N. Rezaei-Ghaleh, F. Klama, F. Munari, M. Zweckstetter, *Angew Chem Int Edit* **2013**, *52*, 11410-11414.